Argonne NATIONAL LABORATORY

ANL-ART-190

Decarburization and Carburization Behavior of Grade 91 Steel in Sodium Environments

Nuclear Science and Engineering Division

About Argonne National Laboratory

Argonne is a U.S. Department of Energy laboratory managed by UChicago Argonne, LLC under contract DE-AC02-06CH11357. The Laboratory's main facility is outside Chicago, at 9700 South Cass Avenue, Argonne, Illinois 60439. For information about Argonne and its pioneering science and technology programs, see www.anl.gov.

ANL-ART-190

Decarburization and Carburization Behavior of Grade 91 in Sodium Environments

Prepared by
Meimei Li and Zuotao Zeng
Nuclear Science and Engineering Division
Argonne National Laboratory

September 2020

ABSTRACT

Two heats of G91 steel have been investigated in sodium at 550- 650°C to understand its corrosion behaviour, microstructural evolution, and tensile properties. Sodium exposure tests of subsized tensile and coupon specimens of G91 base metal and weldment were conducted in Argonne's forced convection sodium materials testing loops. Maximum exposure times of ~39,000 h at 550°C, ~37,000 h at 600°C, and ~20,000 h at 650°C have been achieved, respectively. Thermal aging experiments of G91 steel were conducted in parallel, and the data of the sodium-exposed specimens were compared with the thermal aging data of the same heat to isolate the thermal aging effect from the effect of sodium exposure. It was found that the tensile strength of G91 steel can be reduced by more than 50% after sodium exposures at 650°C. The effect of a sodium environment on tensile properties is largely dependent on the carburization/decarburization behavior of G91 steel exposed to sodium.

The carbon concentrations in sodium in Argonne's SMT-1 and SMT-2 loops were determined by the equilibration method. The carbon activity in sodium was established by equilibrating high-purity nickel in sodium, analyzing the material for carbon, and using the reported data on the carbon solubility for this material. The carbon activity results were combined with the carbon solubility data in sodium to establish the carbon concentration in sodium. The carbon concentrations in the SMT-1 and SMT-2 loop were estimated to be 1.23 and 0.25 ppm, respectively. With this initial success, we will continue to monitor the carbon contents in the two loops to correlate the microstructural and mechanical property changes with the sodium purity. Future experiments will also consider sodium exposure tests in controlled carbon activities. Online monitoring and control of carbon contents in sodium in nuclear reactors would also be of interest.

Thermodynamic analysis was conducted to understand the carburization-decarburization behavior of G91 steel exposed to sodium in the SMT-1 and SMT-2 loops. The equilibrium carbon activity in the alloy was evaluated by the thermodynamics of $M_{23}C_6$ carbides. The calculated carburization-decarburization boundary showed that G91 would undergo decarburization at 650°C in the SMT-1 loop and carburization at 600°C in the SMT-2 loop, which is consistent with our findings from the sodium exposure tests. Future work will include thermodynamic analysis of the carbon concentration – activity relationship including the effect of carbide-forming elements, vanadium and niobium in G91 steel. Kinetics of carbon diffusion and the effect on microstructure and mechanical performance under various service conditions will also be investigated. The ultimate goal is to understand the mechanisms and the kinetics of carbon transfer in the sodium-steel system and to provide a basis for predicting the effect of long-term decarburization-carburization process on the integrity of reactor components.

TABLE OF CONTENTS

LIST OF TABLES

LIST OF FIGURES

1 Introduction

The Advanced Reactor Technologies campaign has focused on the sodium-cooled fast reactor concept because it is a leading candidate for recycling used fuel to close the fuel cycle and because of its technical maturity. The current needs are for more reliable, more flexible, and more economical reactors suitable for commercial nuclear power generation. Research and development addresses three main areas including advanced materials, innovative designs of components and systems, and computer modeling and simulation. Advanced Materials Development Campaign focuses on development and qualification of high-performance advanced materials and understanding and prediction of long-term performance of reactor structural materials that are exposed to the sodium coolant at elevated temperatures.

Figure 1 shows a schematic of a sodium-cooled fast reactor (SFR) [1]. In these reactors, heat is generated from fission reactions in a nuclear-fueled core. The heat is removed by liquid sodium flowing through the core, transferred to a steam system, and the steam is used to drive a turbine. Sodium is an excellent heat transfer medium because of its high thermal conductivity, high heat capacity, and a large liquid temperature range (98-883°C). Sodium as the reactor coolant in SFRs, allows for a high power density with a low coolant volume fraction. Advanced materials are a critical element in the development of next-generation SFRs. Enhanced materials performance not only improves safety margins for component performance and provides design flexibility but is also essential for the economics of advanced SFRs. Structural materials of these reactors will be exposed to harsh operating environments including high temperature, sodium exposure, and neutron irradiation. Degradation due to high temperature and irradiation damage are common issues to all types of reactor materials, while environmental degradation in liquid sodium is unique to SFR materials.

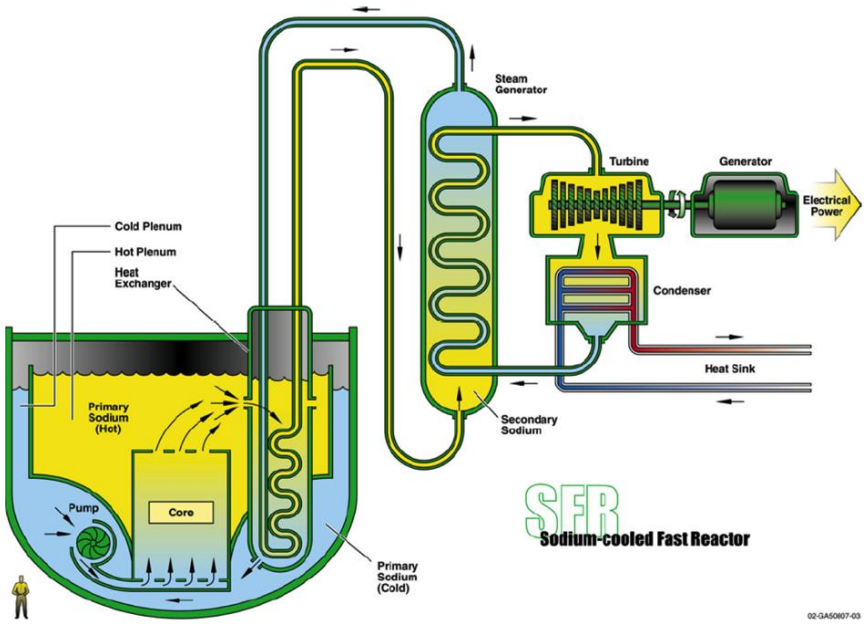

Figure 1. A schematic diagram of a sodium-cooled fast reactor.

Structural materials can undergo a variety of interactions upon exposure to liquid sodium. The interactions can be broadly classified into metallic and nonmetallic element transfer. Metallic element transfer is a solution process of a solid metal in liquid sodium. It can cause dissolution of metallic elements into sodium, or by formation of corrosion products on the metallic surfaces that subsequently erode/spall into the flowing sodium. Metallic element mass transfer usually establishes a go/no-go type of evaluation of an alloy for use as a structural material in a liquid sodium environment. Nonmetallic elements, such as oxygen, carbon, nitrogen, and hydrogen, are known to migrate in structural material/sodium systems under both isothermal or non-isothermal conditions as a result of chemical activity differences. Transfer of these elements also occurs in systems where combinations of materials of different composition are used. From the operation of the SFR standpoint, the oxygen impurity in sodium can be controlled to ~1 ppm which would result in acceptable corrosion of ferrous alloys at the typical operating temperature. The solubility of nitrogen in sodium is low at SFR operating temperatures and its effect on the materials performance may not be significant. On the other hand, carbon transfer in materials-sodium systems can result in carburization or decarburization in an alloy, causing microstructural instability and degradation of its mechanical performance which ultimately affect the lifetime of reactor components. The influence of carbon in sodium on the microstructure and mechanical properties of structural materials is a major concern for their applications in SFRs.

Austenitic stainless steels and ferritic/martensitic steels are the two classes of alloys that are of most interest for structural applications in SFRs. Recent efforts have been focused on advanced high-strength austenitic stainless steels, e.g. 316FR (or 316LN), Alloy 709 (Fe-20Cr-25Ni-1.5Mo-Nb,B,N), and high-Cr ferritic steels, e.g. Grade 91 (also known as Mod. 9Cr-1Mo) (Fe-9Cr-1Mo-V,Nb), Grade 92 (Fe-9Cr-0.5Mo-2W-V,Nb). These advanced alloys have superior high-temperature properties than conventional Types 304 and 316 austenitic stainless steels, Fe-2.25Cr-1Mo ferritic steel. Grade 91 (G91) ferritic-martensitic steel was developed for intermediate heat exchanger and steam generator applications in liquid metal reactors (LMRs) in the late 1970s in the United States. It was selected based on creep strength and microstructural considerations. A development program for G91 steel started in early 1980s, and considerable information was generated through the DOE-sponsored programs and industrial development. An extensive mechanical property database was established in air environment, including tensile, toughness, creep, fatigue, and creep-fatigue properties. The general findings were that the alloy had good mechanical performance for structural applications in LMRs, and was resistant to irradiation swelling. Limited data in sodium have been generated. Long-term testing data in sodium are largely lacking.

During exposure of G91 steel to a sodium environment, the alloy undergoes microstructural changes to reach thermodynamically stable phases as well as carburization or decarburization to equalize the carbon activity between the steel and the sodium. The influence of time-and temperature-dependent migration of carbon in the material from sodium exposure has not been fully understood. Data on the effects of carburization/decarburization on the mechanical properties

of G91 are sparse, and the understanding of carburization/decarburization kinetics is limited. Knowledge of G91 weldment performance in sodium environment is currently lacking. Additional work is required to understand the effects of carburization/decarburization on the microstructural stability and their impact on tensile, creep, fatigue, and creep-fatigue properties of G91 steel.

2 Sodium Exposure Tests of G91 Steel

2.1 Materials and specimens

Base Metal

Two heats of G91 steel were studied, G91-H1 and H30176. A small amount of G91-H1 was available for thermal aging and sodium compatibility studies. The material was in the plate form with a thickness of 0.375". The plate was normalized at 1050°C and tempered at 760°C for 1 h and air cooled. Heat of H30176 was provided by the Oak Ridge National Laboratory and has a relatively large quantity. This heat was in the 1"-thick plate form, and was normalized at 1050°C for 1 h, air cooled, and tempered at 760°C for 2 h and air cooled. The chemical composition and heat treatment conditions of these two heats are given in Tables 1 and 2, respectively.

Table 1. Chemical composition (in wt%)

Heat No.	Fe	C	Cr	Mn	Mo	N	Nb	Si	V	W
G91-H1	Bal	0.09	8.3	0.46	1.04	0.06	0.05	0.41	0.22	-
H30176	Bal	0.08	8.6	0.37	0.89	0.06	0.07	0.11	0.21	<0.01

Table 2. Heat treatment conditions.

Heat No.	Heat treatment
G91-H1	Normalized at 1050°C and tempered at 760°C for 1 h and AC
H30176	Normalized at 1050°C for 1 h, AC, and tempered at 760°C for 2 h, AC

Subsize sheet-type tensile specimens with extended grip sections (Fig. 2 [2]) were used in sodium exposure tests and post-exposure microstructural analysis and tensile tests. The design of extended grip sections was to ensure that microstructural characterization and tensile test were carried out on the sample exposed to the same sodium condition. Tensile specimens were electrical-discharge-machined with the gage parallel to the rolling direction. The tensile specimen has nominal gage dimensions of 0.30 × 0.06 × 0.03 in.

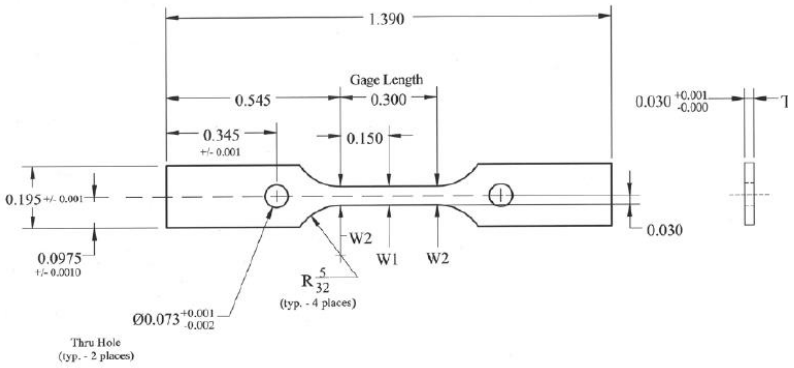

Figure 2. A schematic drawing of subsize sheet-type tensile specimens with extended grip sections for microstructural analysis (unit: inch).

Weldment

Four welded plates of G91 steel were made by Specialty Welding & Machining, LLC., Harrison, TN. The welding procedure conforms the ASME B&PV Section IX requirements. Heat 30176 of G91 steel was used as the base metal. The welded plate had dimensions of 14" L × 6" W × 1" T. The welding process was gas tungsten arc welding (GTAW). The weld wire was ER90S-B9 procured by the vendor with the certificate of analysis. Post-weld heat treatment was conducted at 760°C for 2 hours and air cooling.

Coupon specimens were electrical-discharge-machined from the G91 welded plates. Figures 3 (a) and (b) show a schematic drawing of the coupon specimen, and the fabrication drawing of coupon specimens, respectively. The nominal dimensions of the coupon specimen are 1.40 × 0.20 × 0.04 in.

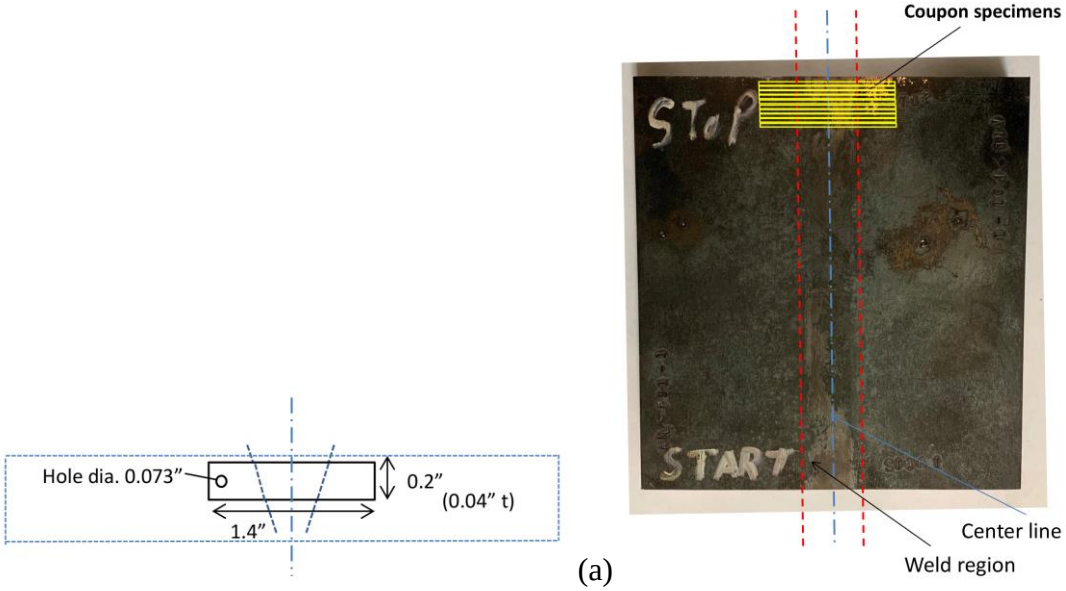

Figure 3. (a) A schematic drawing of coupon specimens and (b) fabrication drawing of coupon specimens made from the G91 weld plate (unit: inch).

2.2 Sodium exposure tests

Sodium exposure tests were performed at 550, 600, and 650°C for G91 base metal, and 550 and 600°C for G91 weldment. Table 3 summarizes the total exposure times at different temperatures for the two heats of G91 base metal and weldment.

Prior to sodium exposure tests, each specimen was weighed three times using an OHAUS Model AP250 analytical balance to a precision of 10 μg. The thickness of the specimen was measured three times using a micrometer to a precision of 0.0001 in. After the sodium exposure test, the specimen was removed from the sodium loop, cleaned with alcohol, and final cleaning with water to remove sodium residues. Specimen surfaces were visually inspected and recorded by a digital camera if needed. Mass and thickness measurements were conducted to determine the mass and thickness changes resulted from sodium exposures. The post-exposure weight and thickness data were compared with the pre-exposure results to evaluate the corrosion performance. If only non-destructive (weight and thickness) measurements were performed on a specimen, the specimen was reloaded into the sodium loop for continued exposure.

Table 3. Sodium exposure temperatures and total exposure times of G91 base metal and weldment.

Heat No.	Total Exposure Time at 550°C (h)	Total Exposure Time at 600°C (h)	Total Exposure Time at 650°C (h)
G91 H1	~30,000	---	~20,000
G91 H30176 base metal	~39,000	~37,000	~10,000
G91 H30176 weldment	~3,000	~4,700	---

Post-exposure destructive examinations included microstructural characterization and tensile tests. The extended grip sections of the exposed tensile specimen were cut from both ends before the tensile test for microstructural analysis. Metallographic specimens were made from the cross section for examination of the specimen surface. Microstructural characterization was conducted by optical microscopy (OM) and high-resolution scanning electron microscopy (SEM). Micro-hardness measurements were conducted on the cross-section specimens to obtain the hardness profiles through the specimen thickness. TEM thin foil specimens were made near the centerline of the specimen thickness by mechanically removing a similar amount of material in the thickness direction from both sides, and electropolishing to perforation using a Tenupol twin-jet polishing unit. TEM specimens were also made by a focused ion beam (FIB) milling technique to life-out samples at a given distance from the exposed surface to examine the depth–dependent microstructure.

Sodium-exposed sheet-type subsize tensile specimens were tested under uniaxial tension at the sodium exposure temperature in an air furnace to examine the effect of sodium exposures on tensile properties. Tensile tests were performed in an electromechanical testing system

equipped with a three-zone air furnace. The applied load was recorded by a load cell. The specimen displacement was measured by the crosshead extension. The engineering tensile properties were determined from analysis of the load and displacement data files. All the tests were conducted at a nominal strain rate, 0.001 s^{-1}.

2.3 Thermal aging tests

Thermal aging experiments were conducted at 550, 600, and 650°C on two heats of G91 steel, G91-H1 and H30176. Thermal aging data of G91 were compared with the sodium exposure data to isolate the thermal effect from the sodium exposure effect. Thermal aging experiments were performed in air furnaces using the same type of specimens shown in Fig. 2. Each specimen was wrapped in Ta foil and encapsulated in a quartz tube under vacuum. Encapsulated specimens were loaded in an air furnace and the furnace was heated to the target temperature for a desired period. Microstructure of the thermally-aged specimens was characterized by optical microscopy (OM), high-resolution scanning electron microscopy (SEM), transmission electron microscopy (TEM), and energy dispersive spectroscopy (EDS). Tensile tests were conducted under uniaxial tension at the aging temperature in an air furnace at a nominal strain rate of 0.001 s^{-1}.

2.4 Experimental Results

The corrosion behavior of ferritic steels is sensitive to changes in temperature, oxygen content in sodium, and sodium velocity [3]. Similar to austenitic stainless steels, after an initial period, the metal-loss rates reach a steady-state value and remain constant with time for given sodium purity and operating conditions. The corrosion behavior of Grade 91 steel was investigated at temperatures of 550, 600, and 650°C in sodium with controlled oxygen content (~1 wppm) in Argonne's forced convection sodium loops. Weight loss was observed at all three temperatures. The corrosion rates decreased with increasing exposure time and reached a steady-state value after ~10,000 h. The initial transient tended to show more variable behavior with relatively large data scatter. The corrosion rates of Grade 91 have an average value of 0.1 μm/y at 550°C, 0.2 μm/y at 600°C, and 0.3 μm/y at 650°C, respectively. It was reported that the corrosion rate increases with an increase in sodium velocity up to ~7 m/s, at which point the corrosion rate becomes velocity independent (Tyzack and Thorley 1978).

The following corrosion formula was used for Monju structural materials in the design [4]:

$$log_{10}R = 0.85 + 1.5log_{10}C_0 - \frac{3900}{(T+273)} \quad (1)$$

where R is the corrosion rate (mm/y), C_0 is the dissolved oxygen (wppm, $5 \leq C_0 \leq 25$ wppm), and T is the temperature (°C, 400°C ≤ T ≤ 650°C). Figure 4 shows the calculated corrosion rates at three different oxygen contents using Eq. (1) and the measured corrosion rate data for Grade 91 in

sodium at the oxygen level of ~1 wppm. The measured corrosion rates were taken for the exposure times of 10,000 – 30,000 h. It appears that the corrosion formula is valid for G91 steel.

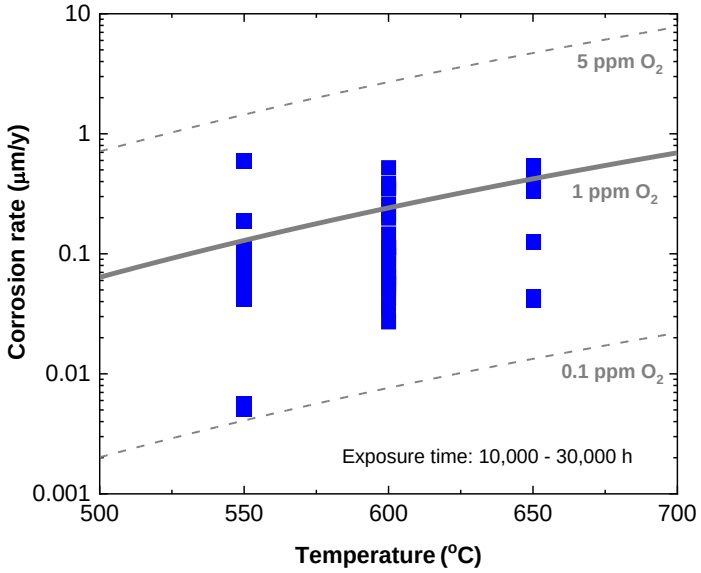

Figure 4. The calculated corrosion rates using the Monju formula and the measured corrosion rate data taken during the exposure times of 10,000 – 30,000 h for G91steel exposed to sodium at 550, 600, and 650°C in Argonne's forced-convection sodium loops.

The effect of a sodium environment on tensile properties is largely dependent on the degree of carburization/decarburization that occur in G91 steel during long-term exposure to sodium. The effect of sodium exposures on the tensile properties of G91 steel was evaluated by conducting post-exposure tensile tests at the sodium exposure temperature. Sodium exposures at 550 and 600°C caused virtually no additional effect on the tensile properties of G91 steel relative to thermal aging under the same temperature and exposure time. In contrast, sodium exposures at 650°C had a drastic effect on its tensile strength. As shown in Fig. 5, the yield stress and the ultimate tensile strength of G91 steel decreased dramatically with increasing exposure time after the initial ~1,000 h and reached a plateau at an exposure time of ~10,000 h. The maximum reductions of the yield stress and the ultimate tensile strength were >50% after sodium exposures. The effect of thermal exposures at 650°C, on the other hand, was much smaller. The maximum reductions of the yield stress and ultimate tensile strength after thermal exposures at equivalent exposure times were <15%. The reduction of tensile strength was accompanied by the recovery of work hardening capacity and the uniform elongation but had minimal effects on the total elongation. Drastic microstructural changes were observed in G91 steel exposed to sodium at 650°C, which explains the drastic reduction in tensile strength [5].

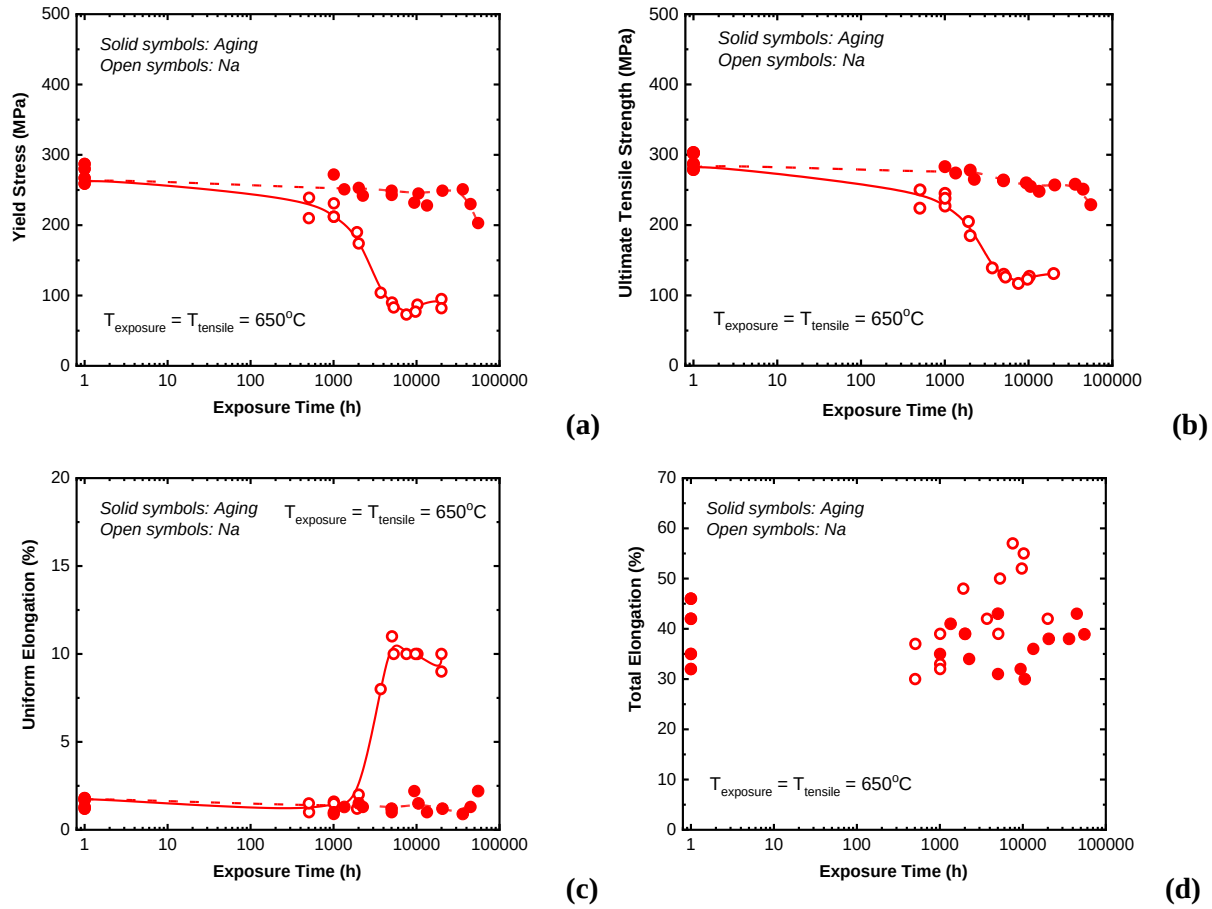

Figure 5. (a) Yield stress, (b) ultimate tensile strength, (c) uniform elongation, and (d) total elongation as a function of exposure time for G91 steel tensile tested at the exposure temperature of 650°C.

3 Measurements of Carbon Contents and Activities in Sodium Loops

Carbon is the key element that determines the mechanical properties of steels. The change of the carbon concentration in G91 during sodium exposure can significantly affect its corrosion rate, microstructural stability, and mechanical properties. The carburization and decarburization behavior of G91 steel depends on both the temperature and the carbon activity in sodium. It is therefore necessary to measure the carbon content in sodium.

The carbon concentration in sodium in Argonne's sodium materials testing loops, SMT-1 and SMT-2 was determined by a foil equilibration method. Equilibration experiments were conducted using pure nickel foil specimens with a thickness of 0.25 mm. Specimens were exposed to sodium at 650°C in the SMT-1 loop, and at 600°C in the SMT-1 loop for times necessary to reach 99% of the equilibrium carbon concentration in nickel. Carbon contents of the equilibrated foil samples were analyzed by a LECO CS-844 carbon analyzer. The carbon activity in sodium

was then obtained, and the carbon concentration in the sodium loops was estimated using the relationship between carbon concentration and carbon activity in sodium. This was the first time the carbon concentrations in these two loops were measured.

3.1 Background

Accurate measurement of carbon concentrations in small-scale loop systems and in reactors is a challenge because of the low carbon activities in sodium. Several techniques have been used to measure carbon concentration in sodium, e.g. foil equilibration method, electrochemical and diffusion-type carbon meters. Of the various techniques, the equilibration method has the greatest potential for achieving accurate measurements of the carbon activity in sodium, in addition to being the simplest and least expensive approach to the problem [6]. The method can also be used as a reliable calibration standard for various type of carbon meters.

The foil equilibration method requires the material has a low corrosion rate in sodium, a sufficient large carbon diffusivity to permit 99% equilibration achieved in a reasonable time, and a large carbon distribution coefficient between the material and sodium [6]. Pure nickel meets such requirements and was chosen for this application. Another advantage of using pure nickel is that it does not form carbide phases.

The time to reach 99% equilibration for carbon diffusion in nickel foils at various temperatures was calculated by Natesan and Kassner [6]. The calculations were reproduced in Fig. 6 where the calculated equilibration times are given as a function of temperature for nickel foils of various thicknesses. From Fig. 6, it can be estimated that for a nickel foil with a thickness of 0.25 mm requires an exposure time of >100 h for carbon to reach 99% equilibration at 650°C, and >300 h at 600°C, respectively. When the carbon concentration reaches equilibration in a nickel foil, the concentration of carbon in nickel can be analyzed by a carbon analyzer.

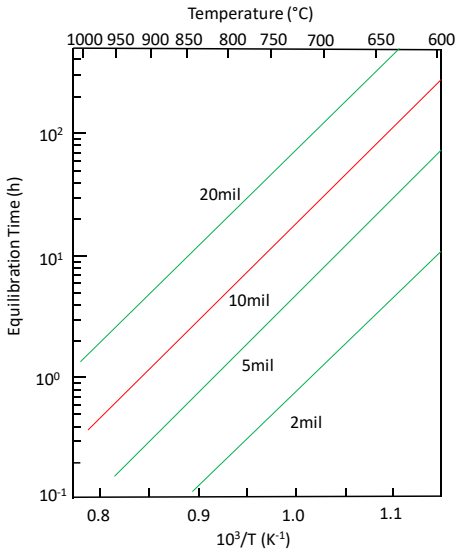

Figure 6. Calculated equilibration time as a function of temperature for carbon diffusion in nickel foil samples of various thicknesses.

The carbon solubility in nickel, S_{Ni} increases with increasing temperature, and it can be expressed as [7]:

$$\frac{S_{Ni}}{1-2S_{Ni}} = exp\left(-\frac{\Delta H}{RT}\right) exp\left(\frac{\Delta S}{R}\right) \quad (2)$$

where ΔH = 9.64 kcal/mol, ΔS = -1.69×10^{-3} kcal/mol/K, R is the gas constant (1.987 cal/mol/K), and T is the absolute temperature, K. The solubility of carbon in nickel was also reported by Lander et al [8], with the relation of:

$$ln(S_{Ni}) = 2.480 - \frac{4880}{T} \quad (3)$$

The solubility of carbon in nickel reported by Natesan and Kassner [9] has the following relationship with the temperature:

$$ln(S_{Ni}) = 2.518 - \frac{5160}{T} \quad (4)$$

Figure 7 shows the calculated carbon solubility in nickel as a function of temperature using the above three models. The Lander model was used in this study, and the carbon solubility in nickel is 0.0446 wt% at 600°C, and 0.0604 wt% at 650°C, respectively.

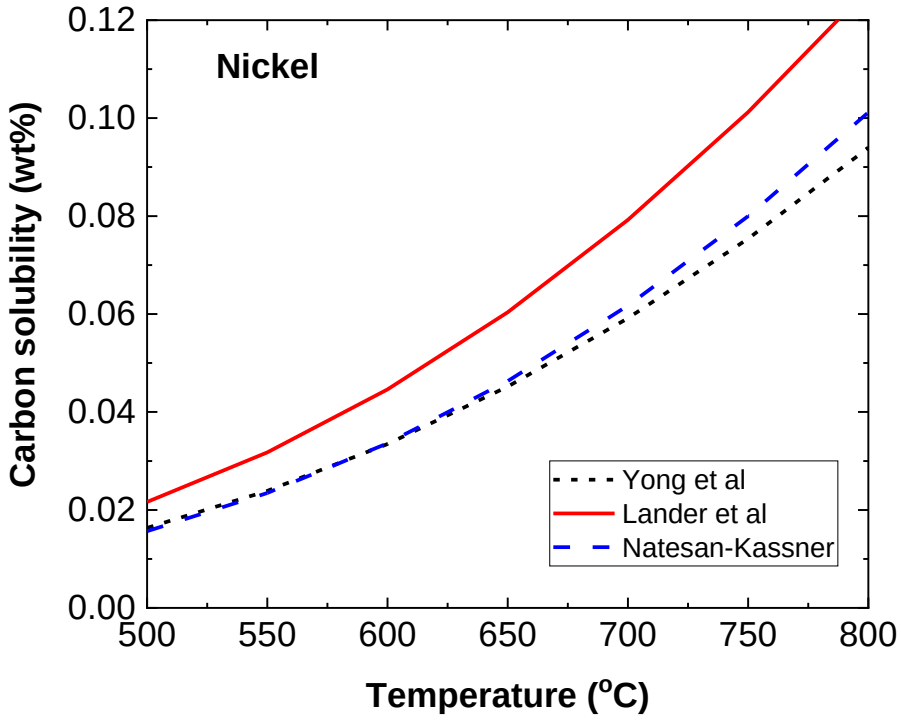

Figure 7. The calculated solubility of carbon in nickel as a function of temperature.

With the values of carbon concentration and solubility in a nickel foil, the carbon activity in nickel, a_{CNi} can be obtained according to Henry's law:

$$a_{C_{Ni}} = \frac{C_{Ni}}{S_{Ni}} \quad (5)$$

where C_{Ni} is the carbon concentration in a nickel foil, and S_{Ni} is the saturated carbon concentration in nickel.

The solubility of carbon in sodium has been studied by Longson and Thorley [10]. The relationship between the carbon solubility in sodium, S_{Na} (ppm) and temperature, T (K) is given as:

$$\log_{10}(S_{Na}) = 7.20 - \frac{5465}{T} \quad (6)$$

Figure 8 shows the carbon solubility in sodium as a function of temperature. Using Eq. (6) it was calculated that S_{Na} = 8.71 ppm at 600°C and S_{Na} = 19.02 ppm at 650°C.

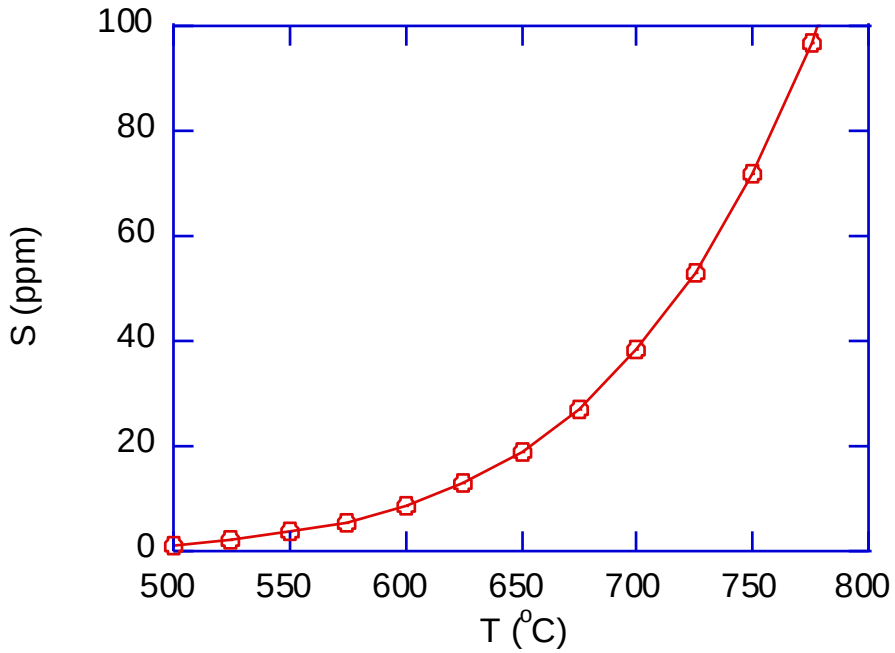

Figure 8. The calculated solubility of carbon in liquid sodium as a function of temperature.

The carbon activity in sodium, a_C can be determined by the following equation [10]:

$$a_{C_{Na}} = \frac{C_{Na}}{S_{Na}} \quad (7)$$

where C_{Na} is the carbon concentration in liquid sodium, and S_{Na} is the saturated carbon concentration in liquid sodium calculated by Eq. (6).

When a nickel foil is exposed to liquid sodium and saturated, the system of sodium with nickel reaches the equilibrium, and the carbon activity in sodium is equal to the carbon activity in nickel, i.e.:

$$a_{C_{Na}} = a_{C_{Ni}} \tag{8}$$

Substituting Eqs. (5) and (7) into Eq. (8), the following equation can be written:

$$\frac{C_{Ni}}{S_{Ni}} = \frac{C_{Na}}{S_{Na}} \tag{9}$$

The concentration of carbon in liquid sodium can therefore be determined by:

$$C_{Na} = S_{Na}\frac{C_{Ni}}{S_{Ni}} \tag{10}$$

If the carbon concentration in nickel is measured, the concentration of carbon in liquid sodium can be obtained.

3.2 Sodium Exposure Experiments of Nickel Foil Specimens

Two forced convection sodium loops were constructed at the Argonne National Laboratory for sodium exposure tests of advanced materials. The Sodium Materials Test Loop 1 (SMT-1) (shown in Fig. 9(a) [2]) consists of a single specimen-exposure vessel with an electromagnetic pump, two electromagnetic flow meters, an economizer, and a cold trap. The total amount of sodium in the loop is approximately 10 kg. The vessel has large penetrations at the top for sample loading as well as small penetrations for a level probe, a thermocouple, and an argon/vacuum line. The maximum operating pressure and temperature of the specimen vessel are 5 psig and 700°C, respectively. The SMT-1 loop has been operating at 650°C.

The Sodium Materials Test Loop 2 (SMT-2) (shown in Fig. 9(b) [11]) is a dual sample-vessel loop for sodium exposure tests at two temperatures. The maximum operating pressure and temperature for the two sample vessels are 5 psig and 700°C, respectively, and the total amount of sodium in the loop is approximately 20 kg. Each vessel has two penetrations at the top for sample loading as well as smaller penetrations for a level probe, thermocouple, and argon/vacuum line. The SMT-2 loop has been running at two temperatures, with one sample vessel at 550°C, and the other at 600°C.

Both loops are constructed of austenitic stainless steels. The oxygen content in sodium is controlled by the cold trap method in both loops. The solubility of oxygen in sodium, *S* can be described by [12]:

$$\log S(wppm\ O) = 6.239 - 2447/T \tag{11}$$

where *T* is the temperature in K. The solubility of oxygen in sodium is ~1 wppm at the cold trap temperature of 125°C.

To measure the carbon concentrations in sodium in the SMT-1 and SMT-2 loops, high-purity (99.999%) nickel foils with the thickness of 0.25 mm was procured from Goodfellow.

Nickel foil specimens were made with nominal dimensions of 10×50×0.254 mm and an approximate total weight of 1.1 g. Foil specimens were exposed to sodium at 600°C in the SMT-2 loop and at 650°C in the SMT-1 loop, respectively. To ensure equilibration was reached, samples were exposed to Na for 1001 h at 600°C, and 3066 h at 650°C. The exposure time is sufficiently long to reach the 99% equilibration.

After the nickel foil samples were removed from the sodium loops, they were cleaned by distilled water and ethanol to remove residual sodium. The carbon contents in the sodium-exposed nickel foil specimens were measured by a LECO CS844 carbon analyzer.

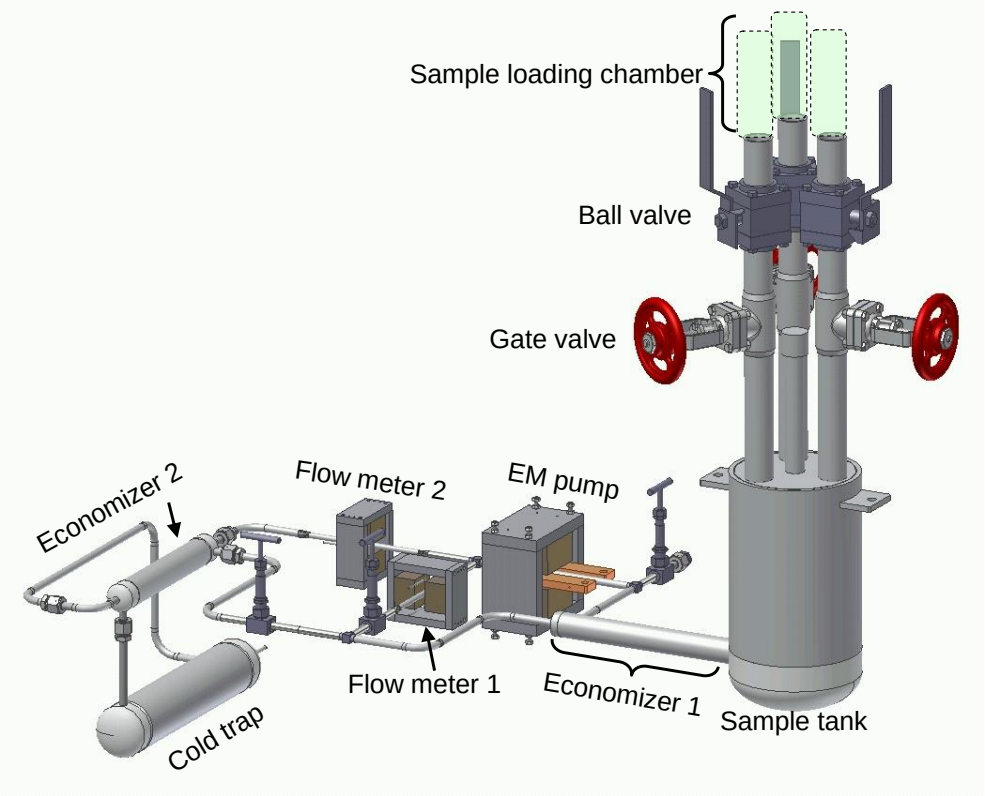

(a)

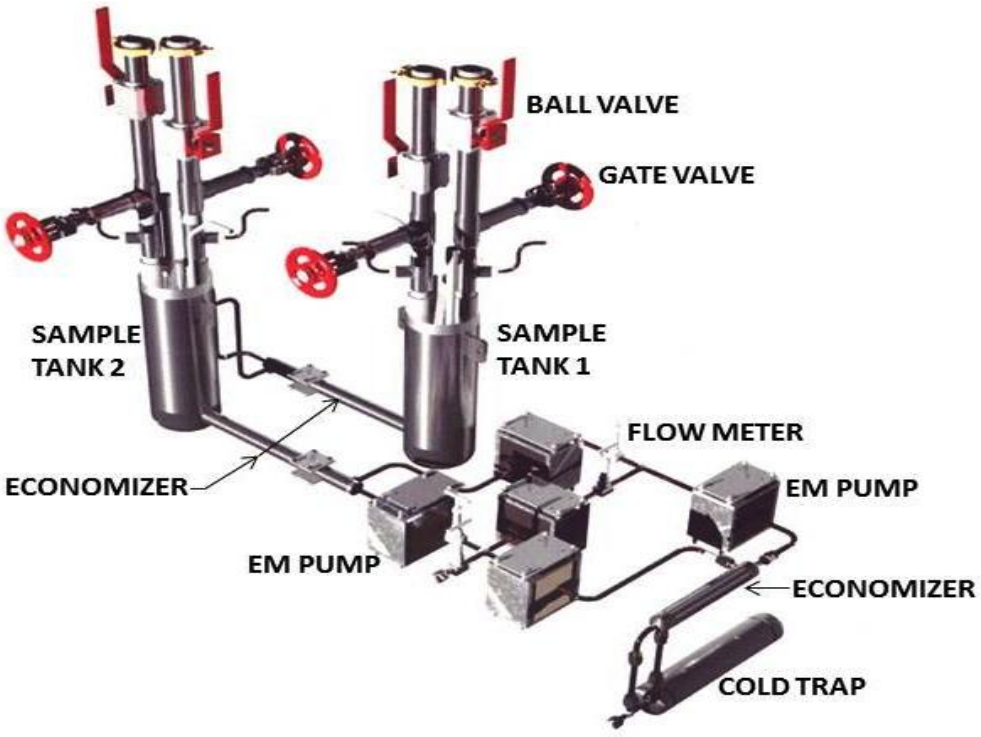

(b)

Figure 9. Isometric view of (a) the Sodium Materials Test Loop 1 (SMT-1) and (b) the Sodium Materials Test Loop 2 (SMT-2).

3.3 Carbon Analysis of Sodium-Exposed Nickel Foil Specimens

Carbon analysis of the equilibrated nickel foil specimens was performed using a LECO CS844 carbon analyzer. The CS844 carbon analyzer utilizes a high-efficiency induction furnace that can quickly break down a sample and allows rapid determination of carbon content in the sample. It has a detection limit of ~0.6 μg per 1 g sample. Sample preparation is an important step before carbon analysis. Surface contamination on the sample can cause significant errors in the carbon analytical data. Care was taken to ensure that a clean, representative sample was analyzed.

The procedure outlined in Application Note #203-821-423 "Carbon and Sulfur in Iron, Steel, Nickel-Base, and Cobalt-Base Alloys" was followed. Analysis was performed utilizing a furnace power setting of 100%, a purge time of 15 seconds, and a delay time of 20 seconds. An integration time of 50 seconds was utilized for carbon determination. For analysis of these specimens, the low carbon calibration was performed utilizing a linear, forced through origin calibrations.

Prior to analysis, all samples were sectioned into ~0.2 g pieces using a benchtop shear, rinsed with acetone to remove any surface contamination, and dried with warm air. All reference materials and prepared samples were weighed into pre-baked LECO 502-018HP High Purity Crucibles, which were previously heated to 1350°C, in a LECO TF-4 for 15 minutes and cooled

in a desiccator. The reference materials and samples were then covered with ~1.2 g LECO 502-173 LECOCEL II HP Accelerator. Table 4 summarized the results of carbon analysis.

Table 4. Carbon analysis results of sodium-exposed nickel foil specimens.

Sample ID	Sample condition	Sample weight (g)	C (wt%)
Ni-650C-9	Na 650°C 3066 h	1.0965	0.0040
Ni-650C-10	Na 650°C 3066 h	0.9782	0.0046
Ni-650C-11	Na 650°C 3066 h	0.9451	0.0032
Ni-600C-4	Na 600°C 1001 h	1.1524	0.0013
Ni-22b	As-received	1.1522	0.0022
Ni-22c	As-received	1.1096	0.0014
Ni-22d	As-received	1.1000	0.0016

The average carbon content in equilibrated nickel foil specimens exposed in the SMT-1 loop was 0.0039±0.007wt%. The carbon content in the nickel foil tested in the SMT-2 loop was 0.0013wt%. It should be noted that several nickel foil samples were exposed to sodium at 600°C in the SMT-2 loop. However, initial carbon analysis of these samples did not give satisfactory results. Only one data was reported in Table 4 for the 600°C-Na-exposed sample. Future equilibration experiments are needed to include more samples in the SMT-2 loop to measure the carbon concentration in sodium.

Based on the measured carbon contents in the equilibrated nickel foil specimens, the carbon concentration in the SMT-2 loop was estimated to be 0.25 ppm, and the carbon concentration in the SMT-1 loop was estimated to be 1.23 ppm. The carbon activity in sodium was calculated using Eqs. (6) and (7) and the results are given in Fig. 10 as a function of temperature for the SMT-1 and SMT-2 loops. The carbon activity in sodium at 650°C in the SMT-1 loop is 0.065, and the carbon activity in sodium at 600°C in the SMT-2 loop is 0.029.

Figure 10 shows that carbon activity in sodium decrease sharply with increasing temperature because of the high solubility of carbon in sodium at high temperature. Sodium tends to create a decarburizing environment at high temperature. The higher carbon concentration in the SMT-1 loop resulted in higher carbon activities in the SMT-1 loop than those in the SMT-2 loop. An alloy is more susceptible to decarburization in sodium with a lower carbon concentration.

A number of factors can affect the accuracy of measured carbon concentrations and activities in sodium: (1) the sensitivity of a carbon analyzer could lead to uncertainty in the measurements of carbon concentration in equilibrated specimens, particularly for low carbon concentrations in the material; (2) the carbon activity in nickel foil samples was calculated based on the ratio of the measured carbon concentration and the solubility of carbon in nickel. Literature

reported different values of the carbon solubility in nickel, and the carbon concentration in sodium can vary depending on the carbon solubility values used; (3) the carbon concentration in sodium was calculated using the solubility of carbon in sodium that can vary significantly depending on the studies. A factor of about five difference in the solubility values of carbon in sodium has been observed [13].

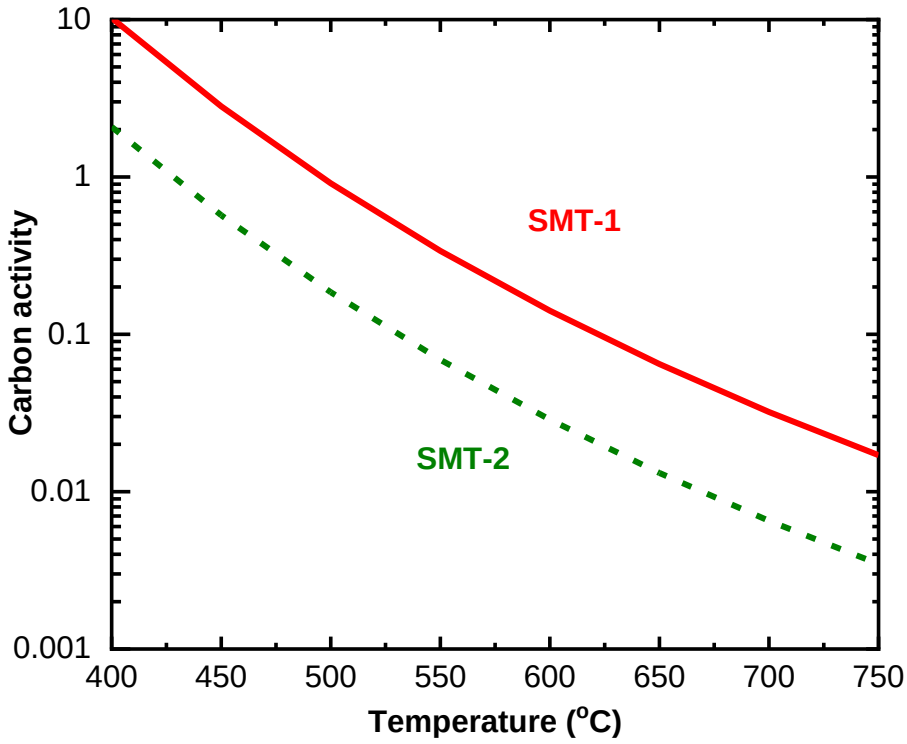

Figure 10. The carbon activity in sodium as a function of temperature in the SMT-1 and SMT-2 loops.

4 Evaluation of Carburization and Decarburization in G91 Steel

4.1 Calculations of Carburization-Decarburization Boundary

Chopra et al. [14] reported the conditions of sodium temperature and carbon concentration that results in either carburization or decarburization of Fe-9Cr-1Mo-0.09C steels, which is given in Fig. 11. The shaded area in Fig. 11 shows the range of carbon concentration in sodium measured for the SMT-1 and SMT-2 loops. According to Fig. 11, G91 steel would carburize at both 600 and 650°C in the SMT-1 and SMT-2 loops. This is inconsistent with our experimental finding that G91 decarburizes at 650°C when exposed to sodium in the SMT-1 loop.

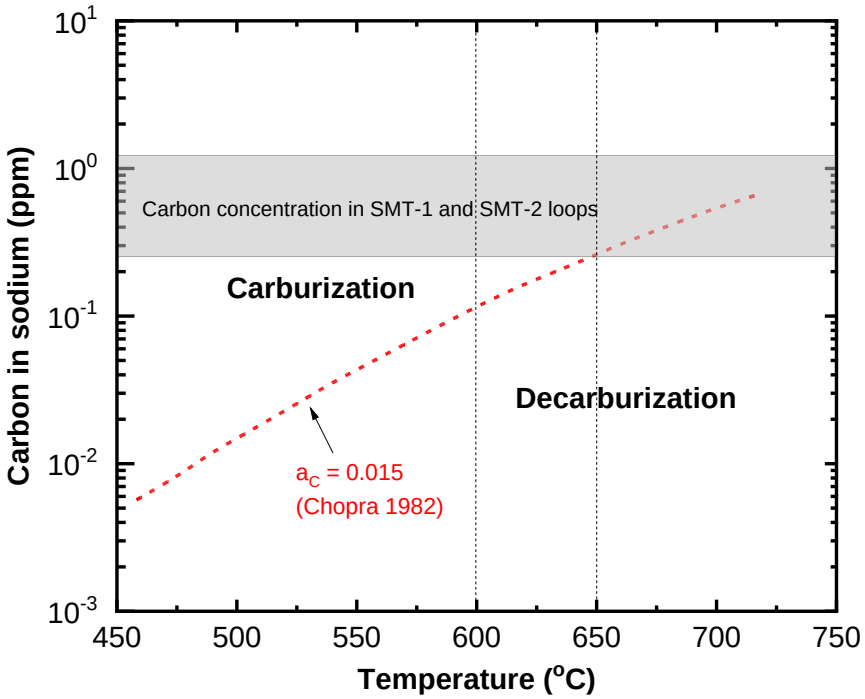

Figure 11. Carburization/decarburization regimes for Fe-9Cr-1Mo steel relative to sodium carbon concentration and temperature reported by Chopra et al [14].

The carburization-decarburization boundary reported by Chopra et al. [14] was determined by assuming a constant carbon activity (0.015) in Fe-9Cr-1Mo steel with a carbon concentration of 0.09 wt%. The carbon activity of the Fe-9Cr-1Mo steel was estimated using the relationship between the equilibrium carbon concentration and activity for the Fe-9Cr-Mo steels determined by equilibration experiments [14]. The results of the equilibration experiments of several high-purity and commercial Fe-9Cr-1 to 2.5Mo steels showed that the equilibrium carbon concentration in Fe-9Cr-Mo steels can be expressed as a function of carbon activity by [14]:

$$C(wt\%) = 0.16a_c^{0.14} + 10.5a_c^{2.2} \quad (12)$$

This equilibrium relationship indicates that the carbon concentration is insensitive to the temperature for a given carbon activity. The crossover temperature of carburization and decarburization in G91 was evaluated assuming a temperature-independent and constant value of the carbon activity, a_c ~0.015, which corresponds to the initial carbon concentration of 0.09 wt% in an Fe-9Cr-Mo steel.

The carbon concentration – activity relationship was calculated using Thermo-Calc software for G91 steel in this work. The results are given in Fig. 12 where the carbon activity in G91 steel was calculated as a function of temperature. The calculation agrees with the result of the carbon activity calculated for P91 using CALPHAD approach by Hodis and Sopousek [15]. The

strong temperature dependence of the carbon activity in G91 calculated by Thermo-Calc is in contrary to the findings reported by Chopra [14] and needs to be understood.

Figure 13 shows the calculated carbon concentration – activity relationship for G91 steel for temperatures of 550, 600, 650, and 700°C with Thermo-Calc software. The results are compared with the study by Chopra et al [14]. There is a significant difference between the calculations and the literature data at low carbon activities. It is known that trace amounts of carbide-forming elements, e.g. V, Nb in the alloy can form stable carbides, decrease the carbon activity coefficient, and hence the carbon activity in the steel. The presence of these elements can significantly influence the carbon concentration – activity relationship of the alloy, particularly at low carbon activities [6]. Future work is needed to understand the difference between the results of the simulation and the equilibration experiments. Accurate determination of the carbon concentration – activity relationship for G91 is critical to the understanding and prediction of the carburization-decarburization behavior of G91 in sodium environments.

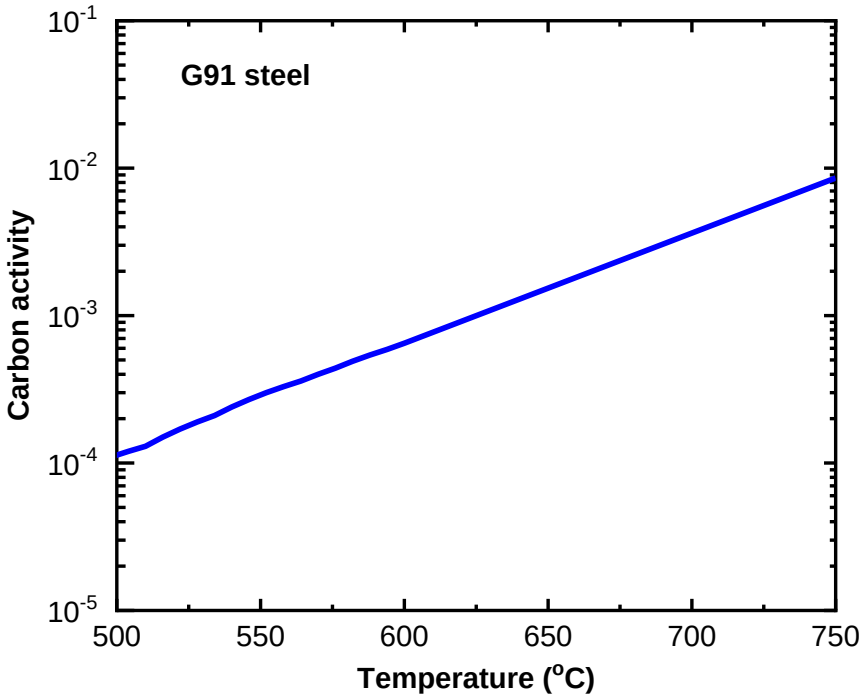

Figure 12. Calculated carbon activity as a function of temperature for G91.

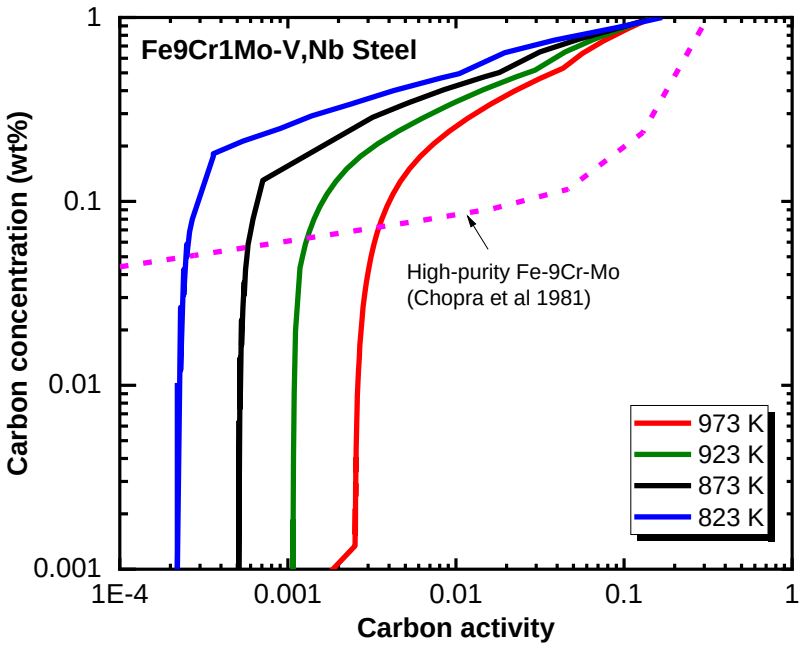

Figure 13. Calculated carbon concentration – activity relationship for G91 steel.

Because the solubility of carbon in the martensite (α-phase) is very low in G91 steel, a majority of carbon exists in carbide phases. The carburization-decarburization boundary may be evaluated by calculating the carbon activity in $M_{23}C_6$ carbides in G91 steel [16]. For the reaction of:

$$\frac{23}{6}Cr + C = \frac{1}{6}Cr_{23}C_6 \tag{13}$$

The equilibrium constant K is given as:

$$K = \frac{a_{Cr_{23}C_6}^{1/6}}{a_{Cr}^{23/6} a_C} = exp\left(-\frac{\Delta G}{RT}\right) \tag{14}$$

The value of free energy, ΔG has been reported in several studies, and the following expression is based on the average values of the reported enthalpy and entropy data, and is used in this study [17]:

$$\Delta G_{Cr_{23}C_6} = -12630 + 2.30T \tag{17}$$

where T is the absolute temperature, K, and the unit of ΔG is cal/g-atom C. The equilibrium constant, K is then expressed as:

$$K = exp\left(-\frac{-12630+2.30T}{RT}\right) \tag{18}$$

where R is the gas constant, 1.987 cal/mol-K.

The $M_{23}C_6$ carbides formed in G91 steel are mixed carbides of $(Fe,Cr,Mo)_{23}C_6$. The composition of carbides changes with temperature. The average composition of the mixed carbides, $Cr_{18}Fe_3C_6$ was used in previous thermodynamic analysis of carbon transfer in Fe-9Cr-Mo steels [17]. The $Cr_{23}C_6$ activity in $M_{23}C_6$ carbides was evaluated using the ideal mixing model. The ideal mixing model assumes that the free energy of mixing in the mixed carbides is due entirely to the entropy of mixing of metallic atoms and there is no contribution from carbon and no heat of mixing. The activity follows a power relationship with mole fraction in the mixed carbides. The ideal mixing model can be applied to solid solutions of carbides where the metal atoms are similar in size and properties [18]. According to the ideal mixing model, the $Cr_{23}C_6$ activity in $Cr_{18}Fe_3C_6$ carbides is given as:

$$a_{Cr_{23}C_6} = \left(\frac{18}{23}\right)^{23} \quad (19)$$

The equilibrium composition of $M_{23}C_6$ in G91 steel at various temperatures was calculated with Thermo-Calc software and the results are given in Table 5. It should be mentioned that all the Thermo-Calc calculations were carried out using the composition of G91 H30176 in this study. The $Cr_{23}C_6$ activity in $M_{23}C_6$ carbides was calculated using the composition given in Table 5.

Table 5. Calculated composition and activity of $M_{23}C_6$ carbides in G91 steel.

Temperature (°C)	$M_{23}C_6$	a_{Cr23C6}
450	Cr18Mo3Fe2C6	3.56×10^{-3}
500	Cr18Mo3Fe2C6	3.56×10^{-3}
550	Cr18Mo3Fe2C6	3.56×10^{-3}
600	Cr17Mo3Fe3C6	9.56×10^{-4}
650	Cr17Mo3Fe3C6	9.56×10^{-4}
700	Cr16Mo3Fe4C6	2.37×10^{-4}
750	Cr15Mo3Fe5C6	5.37×10^{-5}

The Cr activity in α-phase in G91 steel, a_{Cr} was calculated from the relation of:

$$a_{Cr} = \gamma_{Cr} X_{Cr} \quad (20)$$

where γ_{Cr} is the Cr activity coefficient, and X_{Cr} is the mole fraction of Cr in G91 (X_{Cr} = 0.0917). According to Saltelli et al. [17], the chromium activity coefficient of Fe-9Cr-Mo steels can be calculated by:

$$ln(\gamma_{Cr}) = 1.23 + \frac{1204.8}{T} - 9.56 \times 10^{-4} T \quad (21)$$

where T is the absolute temperature (K). The chromium activity coefficient for G91 steel was also calculated by Thermo-Calc, and it is given as:

$$ln(\gamma_{Cr}) = 0.659 + \frac{1594}{T} - 1.14 \times 10^{-3}T \quad (22)$$

The chromium activity in α-phase in G91 steel was calculated using Eqs. (7) and (8), respectively, and the results are compared in Fig. 14.

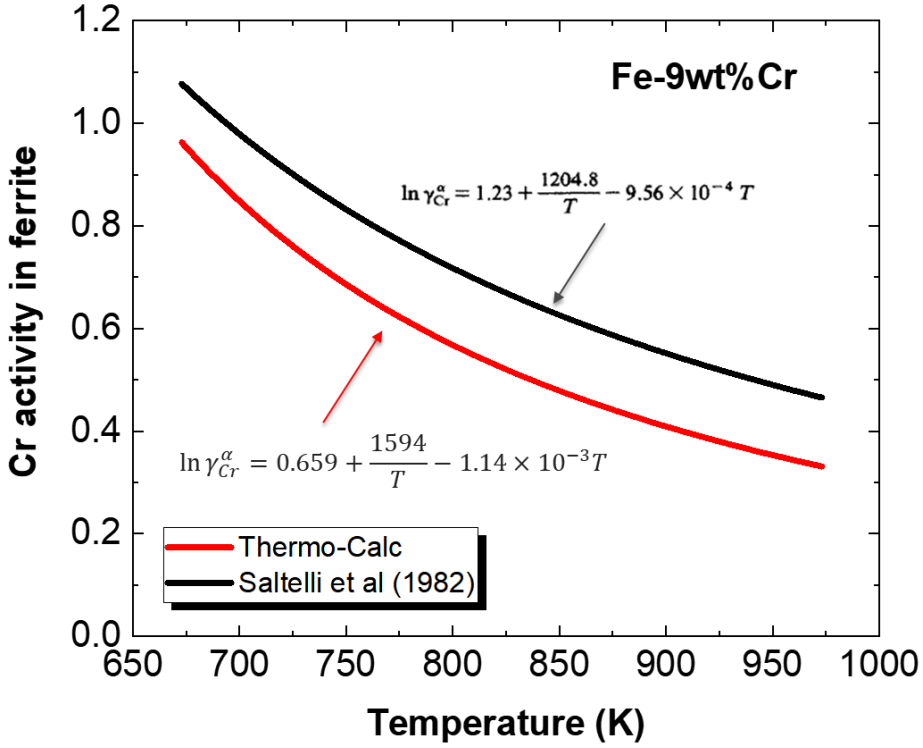

Figure 14. The calculated chromium activity in α-phase as a function of temperature in G91.

Using Eq. (14), the carbon activity of $Cr_{23}C_6$ can be determined by:

$$a_C = \frac{a_{Cr_{23}C_6}^{1/6}}{a_{Cr}^{23/6} \cdot exp\left(-\frac{-12630+2.30T}{RT}\right)} \quad (23)$$

The calculated carbon activity for $Cr_{23}C_6$ in G91 steel is shown in Fig. 15 as a function of temperature. One curve was calculated using the Cr activity coefficient given by Eq. (21), and the other by Eq. (22). It is noted that the carbon activity for $Cr_{23}C_6$ increases with increasing temperature, which implies that $Cr_{23}C_6$ carbides tend to decompose at high temperature. Figure 10 indicates that the carbon activity in sodium decreases with increasing temperature. When the carbon activity in sodium is higher than that of $Cr_{23}C_6$ in an alloy, the carbon will transfer from sodium solution to the alloy. In contrast, if the carbon activity in sodium is lower than that of $Cr_{23}C_6$ in the alloy, the alloy will lose carbon to sodium solution. The crossover temperature of carburization and decarburization in G91 steel can be established by the α-phase and $M_{23}C_6$ isoactivity line, which is given in Fig. 16

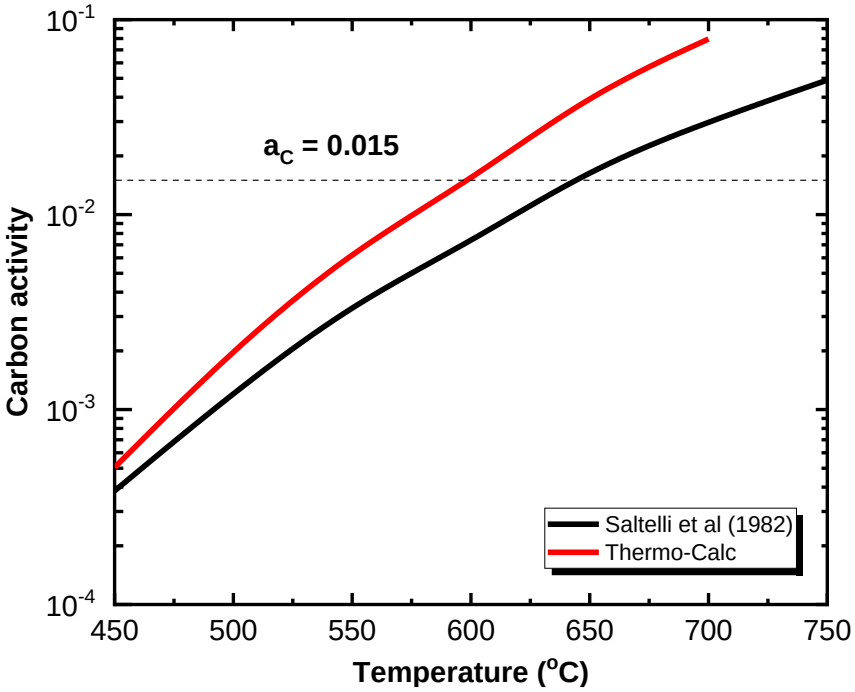

Figure 15. Calculated carbon activity for $Cr_{23}C_6$ in G91 as a function of temperature.

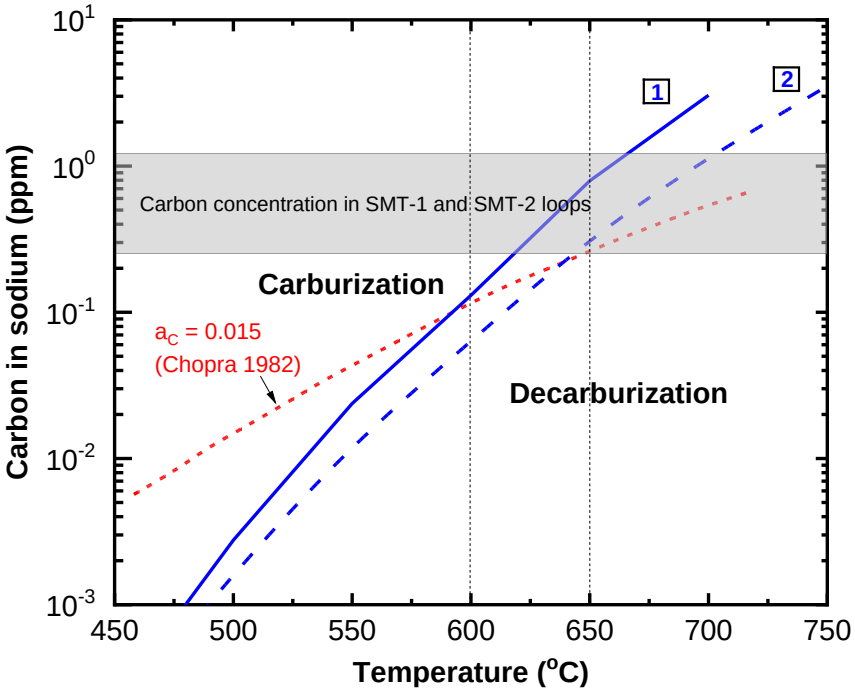

Figure 16. Calculated carburization/decarburization regimes for G91 steel relative to carbon concentration in sodium and temperature.

Figure 16. shows three calculated carburization-decarburization boundaries: (1) boundary calculated by the model developed by Chopra et al [14], (2) boundary labeled as "1" was calculated using the Cr activity coefficient given by Eq. (21), and (3) boundary labeled as "2" was calculated using the Cr activity coefficient given by Eq. (22). The shaded area in Fig. 16 shows the range of carbon concentration in sodium measured in the SMT-1 and SMT-2 loops. Boundary "1" indicates that G91 could decarburize at 650°C in the SMT-1 loop and carburize at 600°C in the SMT-2 loop, which agree with our experimental observations in G91 steel.

4.2 Extrapolation of Sodium Exposure Data to Reactor Environments

It was shown that the crossover temperature between carburization and decarburization of G91 steel is dependent on both the carbon concentration in sodium and sodium temperature. When sodium environments change, the carburization-decarburization response of G91 steel will become different. The crossover temperature for the steel can be lowered significantly when the carbon concentration in sodium environments is lowered. Since carbon concentration in a given system is established by a dynamic equilibrium between carbon sources and carbon sinks present in the system, it could vary from system to system as well as over time within a system. The carbon concentration of sodium in the primary and secondary systems in reactors will depend on the system operating temperature, operating condition, and the materials used to construct the system. Carbon cannot be effectively controlled, unlike oxygen, the level of which can be welled controlled by the cold trap. A quantitative understanding and accurate prediction of the influence of carbon concentration in sodium on microstructure and mechanical properties of G91 steel is of critical importance to the safety and reliability of reactor components.

Figure 17 shows the carburization and decarburization regimes for G91 steel in terms of carbon concentration in sodium and sodium temperature. The boundary shown in Fig. 17 is the boundary "1" in Fig. 16. Also shown in Fig. 17 are the sodium concentrations in sodium in the SMT-1 and SMT-2 loops, in EBR-II primary sodium system, and the dynamic-equilibrium carbon concentration calculated for the FFTF and EBR-II primary systems [19]. According to Snyder et al., the dynamic-equilibrium carbon concentration calculated for the FFTF primary sodium were ~0.025 and ~0.065 ppm for the 474 and 566°C outlet temperatures, respectively, and ~0.018 ppm for the EBR-II primary system if there was no external source of carbon to the system, i.e. other than the carbon initially present in the steel and the sodium. It is noted that the carbon concentration in reactor sodium is significantly lower than those in the sodium loops, which potentially creates a more decarburizing environment. Therefore, the extrapolation of dat obtained in the sodium loops to reactor systems must be done with caution and on a physical basis.

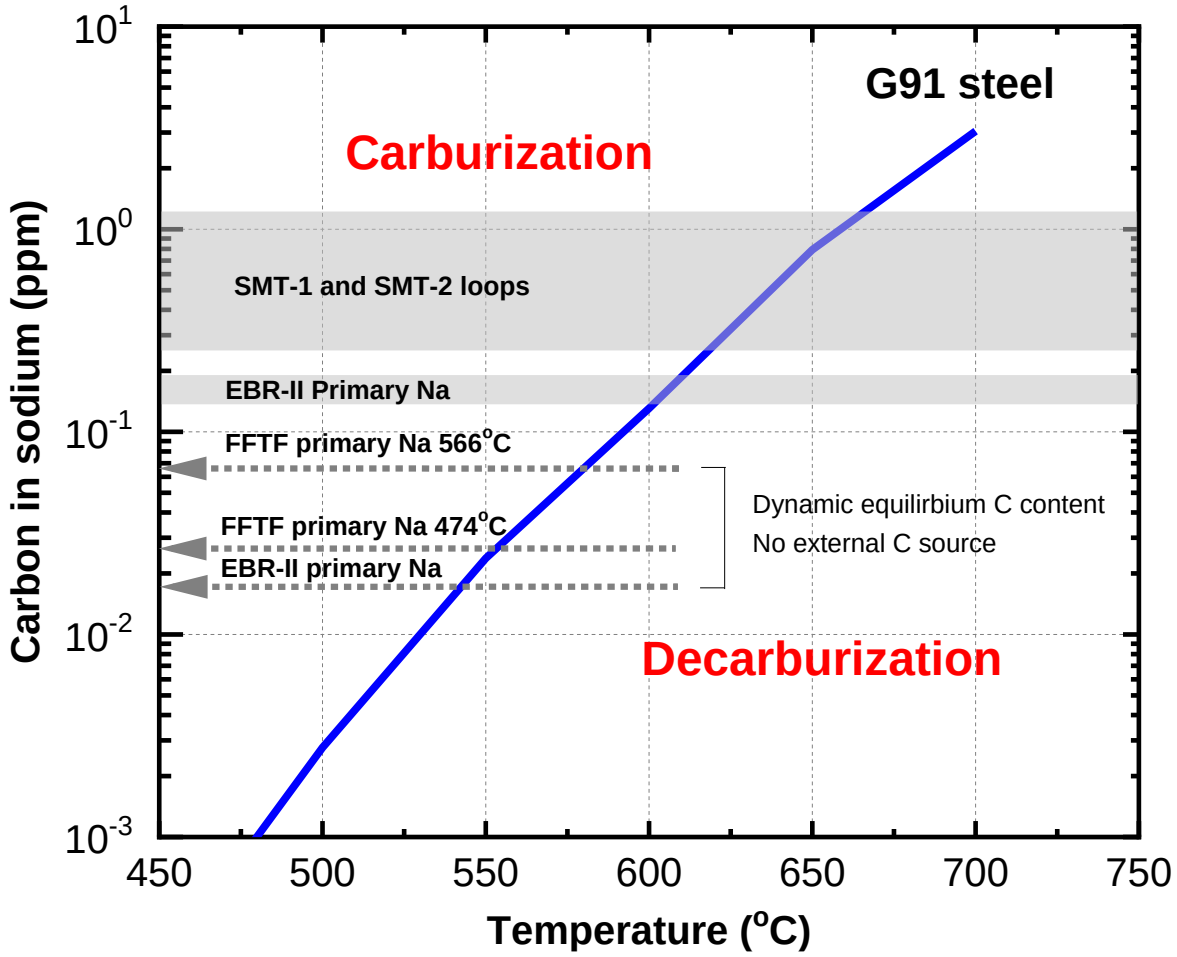

Figure 17. Carburization/decarburization behavior of G91 steel in loop sodium environments and in reactor sodium environments.

5 Summary and Future Work

Two heats of G91 steel have been investigated in sodium at 550- 650°C to understand its corrosion behaviour, microstructural evolution, and tensile properties. Sodium exposure tests of subsized tensile and coupon specimens of G91 base metal and weldment were conducted in Argonne's forced convection sodium materials testing loops. Maximum exposure times of ~39,000 h at 550°C, ~37,000 h at 600°C, and ~20,000 h at 650°C have been achieved, respectively. Thermal aging experiments of G91 steel were conducted in parallel, and the data of the sodium-exposed specimens were compared with the thermal aging data of the same heat to isolate the thermal aging effect from the effect of sodium exposure. It was found that the tensile strength of G91 steel can be reduced by more than 50% after sodium exposures at 650°C. The effect of a sodium environment on tensile properties is largely dependent on the carburization/decarburization behavior of G91 steel exposed to sodium.

The carbon concentrations in sodium in Argonne's SMT-1 and SMT-2 loops were determined by the equilibration method. The carbon activity in sodium was established by equilibrating high-purity nickel in sodium, analyzing the material for carbon, and using the reported data on the carbon solubility for this material. The carbon activity results were combined with the carbon solubility data in sodium to establish the carbon concentration in sodium. The carbon concentrations in the SMT-1 and SMT-2 loop were estimated to be 1.23 and 0.25 ppm, respectively. With this initial success, we will continue to monitor the carbon contents in the two loops to correlate the microstructural and mechanical property changes with the sodium purity. Future experiments will also consider sodium exposure tests in controlled carbon activities. Online monitoring and control of carbon contents in sodium in nuclear reactors would also be of interest.

Thermodynamic analysis was conducted to understand the carburization-decarburization behavior of G91 steel exposed to sodium in the SMT-1 and SMT-2 loops. The equilibrium carbon activity in the alloy was evaluated by the thermodynamics of $M_{23}C_6$ carbides. The calculated carburization-decarburization boundary showed that G91 would undergo decarburization at 650°C in the SMT-1 loop and carburization at 600°C in the SMT-2 loop, which is consistent with our findings from the sodium exposure tests. Future work will include thermodynamic analysis of the carbon concentration – activity relationship including the effect of carbide-forming elements, vanadium and niobium in G91 steel. Kinetics of carbon diffusion and the effect on microstructure and mechanical performance under various service conditions will also be investigated. The ultimate goal is to understand the mechanisms and the kinetics of carbon transfer in the sodium-steel system and to provide a basis for predicting the effect of long-term decarburization-carburization process on the integrity of reactor components.

Acknowledgement

The research was sponsored by the U.S. Department of Energy, under Contract No. DE-AC02-06CH11357 with Argonne National Laboratory, managed and operated by UChicago Argonne LLC. Programmatic direction was provided by the Office of Nuclear Reactor Deployment of the Office of Nuclear Energy (NE).

The authors gratefully acknowledge the support provided by Brian Robinson of DOE-NE, Federal Manager, Advanced Reactor Technologies (ART) Program, Fast Reactors Campaign, Sue Lesica of DOE-NE, Federal Manager, ART Advanced Materials, Robert Hill of Argonne National Laboratory (ANL), National Technical Director, ART Fast Reactors Campaign, and T.-L. Sham of ANL, Technology Area Lead, ART Advanced Materials.

Materials were provided by the Oak Ridge National Laboratory. D. L. Rink is thanked for loop operation, specimen preparation, post-exposure handling, and weight and dimension measurements. Joe Listwan is thanked for conducting tensile tests.

References

[1] https://en.wikipedia.org/wiki/Sodium-cooled_fast_reactor.

[2] Meimei Li, K. Natesan, Y. Momozaki, D. L. Rink, W. K. Soppet, andJ. T. Listwan, ANL-ARC-205, September 2011.

[3] Tyzack, C., A. W. Thorley, Proc. Intl. Conf. on Ferritic Steels for Fast Reactor Steam Generators, BNES, London, p. 241 (1978).

[4] Furukawa, T., E. Yoshida, Material Performance in Sodium, in: R.J.M. Konings (Ed.) Comprehensive Nuclear Materials, Elsevier, Amsterdam, 2012, p. 327.

[5] M. Li, W. Chen, Z. Zeng, Y. Momozaki, ANL-ART-169, Argonne National Laboratory, September 2019.

[6] K. Natesan and T. F. Kassner, Nucl. Tech. 19 (1973) 46.

[7] R. T. Yang, P. J. Goethel, J. M. Schwartz, C. R. F. Lund, J. Catalysis, 122 (1990) 206.

[8] J. J. Lander, H. E. Kern, A. L. Beach, J. App. Phys. 23 (1952) 1305.

[9] K. Natesan and T. F. Kassner, Metall. Trans. 4 (1973) 2557.

[10] B. Longson and A. W. Thorley, J. Appl. Chem., 20, 372-379, 1970.

[11] Unpublished information.

[12] Eichelberger, R. L. Atomics International: Canoga Park, CA, 1968; AI-AEC-12685.

[13] R. B. Snyder, K. Natesan and T. F. Kassner, J. Nucl. Mater. 50 (1974) 259.

[14] O. K. Chopra, K. Natesan, and T. F. Kassner, J. Nucl. Mater. 96 (1981) 269.

[15] Z. Hodis and J. Sopousek, Defect and Diffusion Forum 263 (2007) 225.

[16] S. R. Pillai and C.K. Mathews, J. Nucl. Mater. 150 (1987) 31.

[17] A. Saltelli, O.K. Chopra, K. Natesan, J. Nucl. Mater. 110 (1982) 1.

[18] K. Natesan and T. F. Kassner, ANL-7646, Argonne National Laboratory, 1969.

[19] R.B. Snyder, K. Natesan, T. F. Kassner, International Conference on Liquid Metal Technology in Energy Production, 1976.

Nuclear Science and Engineering Division
Argonne National Laboratory
9700 South Cass Avenue
Lemont, IL 60439

www.anl.gov